
Structured Neural Marked Point Processes for Interpretable Event Interaction Modeling

Zhitong Xu¹, Qiwei Yuan¹, Yinghao Chen¹, Shandian Zhe^{1,2}, and Bin Shen²

¹ Kahlert School of Computing, University of Utah

² Celonis AI

Abstract

Multi-class event streams arise in numerous real-world applications, where uncovering structured, interpretable inter-event relationships, together with accurate prediction, remains a central challenge. Existing neural point process models are highly expressive but encode event interactions in a black-box manner, preventing explicit discovery of structured dependencies. In this paper, we propose a structured neural marked point process (SNMPP) that achieves high modeling flexibility while enabling explicit event-wise and class-wise relationship discovery from data. Our model constructs a product-form neural influence kernel composed of a signed interaction network over event types and a delay-aware monotonic temporal network. This design enables explicit characterization of inter-class influence topology — including excitation, inhibition, and neutrality — while flexibly capturing diverse temporal decay patterns and potential influence delays. For efficient learning, we develop a stratified Monte Carlo estimator for stochastic training. Extensive experiments on synthetic and real-world benchmark datasets validate the ability of our approach to uncover structured relationships and deliver strong predictive performance.

1 Introduction

Multi-class event streams arise in many real-world scenarios, including social networks, online retail platforms, supply-chain systems, medical visit records, and enterprise processes. Modeling such event sequences to uncover structured inter-event dependencies and enable accurate prediction is central to understanding the dynamics of event occurrences. Reliable prediction further supports risk monitoring, early warning, and timely intervention.

Many temporal point process models have been proposed for event modeling. Classical Poisson processes assume event independence and therefore ignore interactions between events. Hawkes processes [Hawkes, 1971] extend this framework by allowing past events to excite future occurrences through parametric triggering kernels, such as the exponential kernel. However, standard Hawkes models are restricted to excitatory effects and do not capture inhibition. Moreover, most formulations assume that an event’s influence is strongest immediately after its occurrence and then decays over time. In many real-world applications, however, event influences may exhibit delayed effects, initially weak and peaking after a certain time lag, as observed in delayed medical treatment effects [Holford, 2018, Meng et al., 2021] or supply-chain replenishment processes [Heydari et al., 2009, Chang and Lin, 2019].

Recent neural point processes have emerged as a dominant framework for event modeling. These models directly parameterize the conditional intensity using deep neural network architectures. For example, the Neural Hawkes Process (NHP) [Mei and Eisner, 2017] and Recurrent Marked Temporal Point Process (RMTTP) [Du et al., 2016] encode event histories via recurrent neural networks and model the intensity as a transformation of the hidden states. The Transformer Hawkes Process

(THP) [Zuo et al., 2020] and Self-Attentive Hawkes Process (SAHP) [Zhang et al., 2020] treat events as tokens and employ causal self-attention mechanisms to obtain contextualized embeddings for intensity computation. Although these approaches substantially enhance representational capacity, event relationships are encoded implicitly within latent representations, hindering explicit and interpretable characterization of interaction structure.

To address these limitations, we propose SNMPP, a structured neural marked point process. Our framework achieves high modeling flexibility while enabling explicit discovery of event-wise and class-wise interaction relationships from data. Our major contributions are as follows:

- **Model.** We construct a product-form neural influence kernel composed of a signed interaction network and a delay-aware monotonic temporal network. The signed interaction network takes pairs of event-type embeddings as input and outputs a signed interaction strength, reflecting the influence topology between event types — including excitation, inhibition, and neutrality. The temporal network is designed to be monotonically decreasing with outputs constrained to the bounded range $[0, 1]$, focusing on modeling the temporal decay of influence. To ensure monotonicity, we incorporate input negation, nonnegative network weights, monotonic activation functions, and soft output clipping. The temporal input is defined as the absolute time difference offset by a learnable delay parameter, enabling the model to capture both delayed peak effects and flexible decay patterns over time.
- **Algorithm.** For efficient training, we develop a stratified Monte Carlo sampling scheme to provide an unbiased estimator of the likelihood integral terms. Specifically, each inter-event interval is partitioned into multiple segments, from which one sample is drawn per segment to estimate the integral. This stratification reduces variance while preserving sensitivity to local variations in the intensity function.
- **Experiments.** We first evaluated SNMPP on two synthetic temporal point process datasets featuring delayed triggering and inhibitory interactions. Our method accurately recovers the conditional intensities, inter-class influence topology, delay parameters, and influence kernel shapes. We next assessed the predictive performance of SNMPP on five real-world benchmark datasets. Our model consistently improves next-event time prediction while achieving competitive event-type prediction accuracy compared to state-of-the-art neural point process models. Finally, we examined SNMPP on a simulated supply-chain system governed by physical constraints, decision rules and stochastic dynamics, rather than a predefined point process model. Despite the non-point-process data-generating mechanism, our method successfully uncovers the induced interaction structure, delayed effects, and gating behaviors underlying the simulation, while accurately recovering critical lead-time parameters.

2 Preliminaries: Marked Temporal Point Processes

We consider a temporal point process with K event types (marks). Let $\mathcal{H}_t = \{(t_n, k_n) : t_n < t\}$ denote the event history up to time t , where t_n is the time of the n -th event and $k_n \in \{1, \dots, K\}$ is its mark. The marked conditional intensity function for type k is defined as

$$\lambda_k(t | \mathcal{H}_t) = \lim_{\Delta t \rightarrow 0} \frac{\mathbb{P}(\text{an event of type } k \text{ occurs in } [t, t + \Delta t] | \mathcal{H}_t)}{\Delta t}.$$

The total conditional intensity is $\lambda(t | \mathcal{H}_t) = \sum_{k=1}^K \lambda_k(t | \mathcal{H}_t)$. The conditional probability that the next event at time t has mark k is $\mathbb{P}(k | t, \mathcal{H}_t) = \frac{\lambda_k(t | \mathcal{H}_t)}{\lambda(t | \mathcal{H}_t)}$.

Let $\Gamma = \{(t_n, k_n)\}_{n=1}^N$ be a sequence of marked events observed over $[0, T]$. The log-likelihood of the observed sequence Γ under the model is

$$\log p(\Gamma) = \sum_{n=1}^N \log \lambda_{k_n}(t_n | \mathcal{H}_{t_n}) - \int_0^T \lambda(t | \mathcal{H}_t) dt.$$

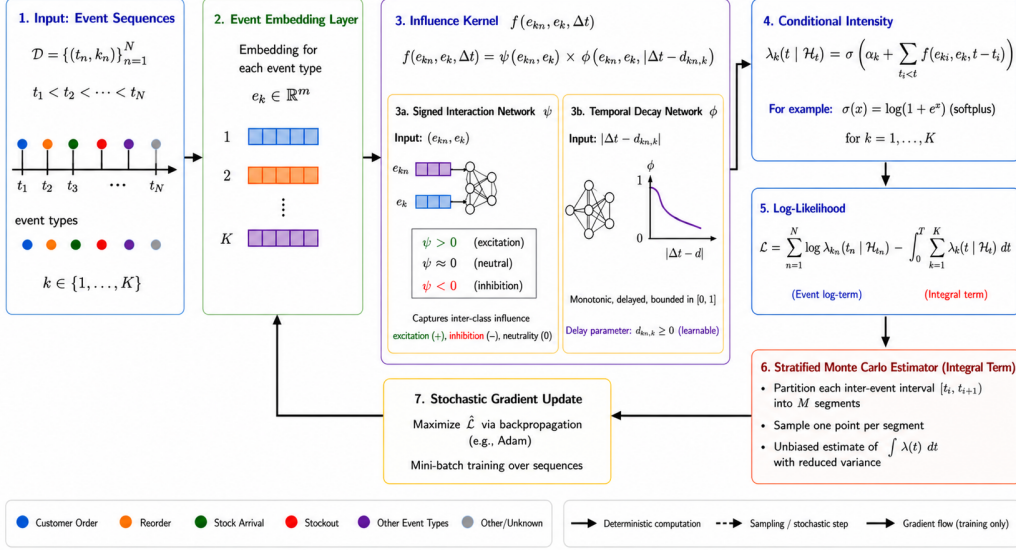


Figure 1: Graphical Illustration of SNMPP.

3 Methodology

3.1 Model

To enable explicit event-wise and type-wise interaction discovery while retaining flexibility to capture complex temporal dependencies, we model the marked conditional intensity as

$$\lambda_k(t | \mathcal{H}_t) = \sigma \left(\alpha_k + \sum_{t_n < t} f_{k_n \rightarrow k}(t - t_n) \right), \quad (1)$$

where α_k is a latent baseline parameter capturing the spontaneous tendency of event type k , and $f_{k_n \rightarrow k}(\Delta t)$ denotes the influence kernel that characterizes how a past event of type k_n affects the intensity of type k events after a time lag $\Delta t = t - t_n$. A positive value of $f_{k_n \rightarrow k}(\Delta t)$ indicates excitation, a negative value indicates inhibition, and values close to zero correspond to negligible influence. To ensure non-negativity of the conditional intensity, we apply a positive link function $\sigma(\cdot)$ to the superposition of the baseline and interaction terms.

Next, we introduce a learnable embedding representation $\mathbf{e}_k \in \mathbb{R}^m$ for each event type k , and model the influence kernel as a function of the corresponding embeddings and the time lag: $f_{k_n \rightarrow k}(\Delta t) = f(\mathbf{e}_{k_n}, \mathbf{e}_k, \Delta t)$. This framework enables a unified modeling of interactions across all event types, requiring only a single function f to capture pairwise influences. In contrast to learning K^2 separate kernels for each ordered type pair, our embedding-based framework reduces model complexity and improves scalability, particularly when the number of event types K is large.

To explicitly capture both type-wise interaction structure and event-wise temporal influence in a flexible and data-driven manner, we further decompose the influence kernel as a product of two neural components:

$$f(\mathbf{e}_{k_n}, \mathbf{e}_k, \Delta t) = \psi(\mathbf{e}_{k_n}, \mathbf{e}_k) \cdot \phi(\mathbf{e}_{k_n}, \mathbf{e}_k, |\Delta t - d_{k_n, k}|). \quad (2)$$

Here, $\psi(\mathbf{e}_{k_n}, \mathbf{e}_k)$ is an interaction network that takes the embeddings of the source and target event types as input and outputs a signed magnitude representing the overall interaction strength and polarity. A positive value indicates excitation (i.e., a triggering effect), a negative value indicates inhibition, and a value near zero corresponds to negligible interaction. The magnitude reflects the maximal influence strength between the two event types. This formulation allows ψ to induce an asymmetric interaction topology among event types, capturing directed relationships without requiring separate parameterizations for each ordered pair.

The network $\phi(\mathbf{e}_{k_n}, \mathbf{e}_k, \Delta t)$ in (2) serves as a temporal kernel that models how interaction strength evolves over time. The embeddings of the source and target event types provide *contextual information*, while ϕ focuses on capturing temporal variation. It is natural to assume that the influence of

past events attenuates over time. To flexibly model a broad class of decay patterns beyond restrictive parametric forms (e.g., exponential decay), we construct ϕ as a *monotonically decreasing* neural network with respect to the time lag.

Specifically, we adopt a feed-forward architecture in which all linear-layer weights are constrained to be non-negative and activation functions are chosen to be monotonically non-decreasing (e.g., Tanh or SoftPlus). By the chain rule, the resulting network is monotonic non-decreasing with respect to its input. To obtain a monotonically *decreasing* function in Δt , we feed $-\Delta t$ into the first layer, ensuring $\frac{\partial \phi}{\partial \Delta t} < 0$.

To ensure that ϕ captures only temporal variation — leaving the overall interaction magnitude and sign to the ψ network — we restrict its output to a bounded interval $[a, b]$. This separation avoids scale confounding between the two neural components and improves interpretability of the learned interactions. While hard clipping via $x \mapsto \min(\max(x, a), b)$ enforces this constraint, it blocks gradients when the output falls outside the interval, potentially hindering optimization. Instead, we use a differentiable soft-clipping transformation:

$$\text{clip}_s(x; a, b) = s \log(e^{x/s} + e^{a/s}) - s \log(e^{(x-b)/s} + 1), \quad (3)$$

where $s > 0$ controls smoothness. As $s \rightarrow 0$, this function converges to $\min(\max(x, a), b)$. A detailed derivation of this smooth approximation, including its connection to log-sum-exp relaxations of the max/min operators and its convergence analysis, is provided in Appendix A. It is natural to set $a = 0$ and $b = 1$, so that the temporal response is constrained to $[0, 1]$, allowing ϕ to capture normalized temporal variation while leaving the overall magnitude and sign to ψ .

To capture delayed effects that commonly arise in practical applications — such as delayed medical treatment responses, replenishment cycles in supply chains, and policy interventions in crime reduction — we introduce a delay parameter $d_{k_n, k} > 0$ representing the peak time of influence. Specifically, we feed $|\Delta t - d_{k_n, k}|$ into the ϕ network, as shown in (2). This formulation allows the influence to be initially weak, increase to its maximum at $d_{k_n, k}$, and decay thereafter, yielding a unimodal temporal profile centered at $d_{k_n, k}$. The model naturally subsumes the non-delayed case as a special instance: when $d_{k_n, k}$ approaches zero, the influence peaks at the event occurrence time.

3.2 Algorithm

Given a collection of observed event sequences \mathcal{D} , training maximizes the joint log likelihood, $\log p(\mathcal{D}) = \sum_{\Gamma \in \mathcal{D}} \log p(\Gamma)$. For each sequence $\Gamma = \{(t_n, k_n)\}_{n=1}^N \in \mathcal{D}$, the log likelihood is

$$\log p(\Gamma) = \sum_{n=1}^N \log \lambda_{k_n}(t_n | \mathcal{H}_{t_n}) - \sum_{k=1}^K \sum_{n=0}^N \int_{t_n}^{t_{n+1}} \lambda_k(t | \mathcal{H}_t) dt, \quad (4)$$

where $t_0 = 0$ and $t_{N+1} = T$. Since no events occur within each inter-event interval (t_n, t_{n+1}) , the history remains unchanged over that interval. By our definition $\mathcal{H}_t = \{(t_i, k_i) : t_i < t\}$, for any $t \in (t_n, t_{n+1})$ we have $\mathcal{H}_t = \mathcal{H}_{t_{n+1}}$. Consequently, the intensity is piecewise-defined and depends only on $\mathcal{H}_{t_{n+1}}$ within each interval.

The integral terms do not admit closed-form solutions. To address this, we propose a stratified Monte Carlo estimator for each interval. Specifically, for each interval $[t_n, t_{n+1}]$, we partition it into Q equal, non-overlapping subintervals S_1, \dots, S_Q such that $\bigcup_{q=1}^Q S_q = (t_n, t_{n+1})$. We then draw one sample \hat{t}_q uniformly from each segment S_q and approximate the integral as

$$\int_{t_n}^{t_{n+1}} \lambda_k(t | \mathcal{H}_t) dt = \int_{t_n}^{t_{n+1}} \lambda_k(t | \mathcal{H}_{t_{n+1}}) dt \approx \frac{t_{n+1} - t_n}{Q} \cdot \sum_{q=1}^Q \lambda_k(\hat{t}_q | \mathcal{H}_{t_{n+1}}). \quad (5)$$

Compared to drawing Q i.i.d. samples uniformly from the entire interval, the stratified estimator remains unbiased while typically reducing variance. Stratification removes the between-segment variance component present in uniform sampling and retains only within-segment variability, which is typically smaller when the intensity varies across the interval. We provide a formal variance-reduction analysis in Appendix B, Lemma B.1. By enforcing coverage across subintervals, it prevents sample concentration in small regions and better captures local variations of the intensity function.

We employ mini-batch stochastic training. At each iteration, a mini-batch of event sequences is sampled from \mathcal{D} , and stratified Monte Carlo sampling is performed to approximate the integral terms for all inter-event intervals within the batch. Model parameters are optimized using stochastic gradient-based optimization. The overall method is illustrated in Figure 1.

4 Related Work

A rich body of work has been developed for temporal point processes. Early models include Poisson processes [Lawless, 1987, Grandell, 2006] and their extensions in matrix and tensor factorization settings [Charlin et al., 2015, Gopalan et al., 2014, 2015]. Hawkes processes (HPs) [Hawkes, 1971] subsequently gained significant attention due to their ability to capture mutual excitation among events [Blundell et al., 2012, Du et al., 2015, Wang et al., 2017, Yang et al., 2017, Xu et al., 2018].

More recently, neural point processes have emerged as a dominant framework for temporal event modeling. These models use deep neural architectures to parameterize the conditional intensity directly. For example, Recurrent Marked Temporal Point Processes (RMTTPP) [Du et al., 2016] employ recurrent neural networks (RNNs) to encode event histories into hidden states, from which the total intensity and mark distribution are derived. Neural Hawkes Processes (NHP) [Mei and Eisner, 2017] follow a related recurrent formulation but use continuous-time LSTM states [Hochreiter and Schmidhuber, 1997] to model marked conditional intensities. Omi et al. [2019] proposed modeling the cumulative intensity function with monotonic networks [Sill, 1997] conditioned on RNN states, thereby avoiding explicit numerical integration in likelihood computation. Subsequent works, including Transformer Hawkes Processes (THP) [Zuo et al., 2020], Self-Attentive Hawkes Processes (SAHP) [Zhang et al., 2020], and Attentive Neural Hawkes Processes (AttNHP) [Yang et al., 2022], treat events and their types as tokens and apply causal attention mechanisms to encode historical dependencies. The conditional intensity is then modeled as a transformation of the resulting contextual representations. More recently, Yuan and Fang [2025] proposed decomposing a point process into the superposition of a classical structured point process, such as a Hawkes process, and a neural point process. This design captures some predefined event structures while assigning the remaining unexplained dynamics to a black-box neural component.

There has also been a growing line of work on intensity-free generative models for temporal event generation, which move beyond the conventional point process likelihood framework [Shchur et al., 2020, Lin et al., 2022, Lüdke et al., 2023, 2026, Kerrigan et al., 2026]. These methods are highly flexible for generation, but they do not directly provide calibrated conditional intensities or explicit event-structure discovery. Finally, Xue et al. [2024] introduced an open-source benchmarking framework that implements many state-of-the-art neural point process models, providing a standardized platform for comparison and evaluation. In contrast to these approaches, our method preserves the flexibility of neural point processes while introducing an explicit neural influence kernel for interpretable event-wise and class-wise interaction modeling.

5 Experiments

5.1 Synthetic Data

We first evaluated SNMPP on synthetic datasets to validate its ability to capture different influence types and interaction patterns. We constructed two temporal point processes:

PP1 consists of two event types, denoted as E_1 and E_2 . E_1 events occur at a constant rate and exhibit a delayed triggering effect on E_2 events:

$$\lambda_{E_1}(t|\mathcal{H}_t) = 0.5, \quad \lambda_{E_2}(t|\mathcal{H}_t) = 0.05 + \sum_{t_n < t, k_n = E_1} 0.6 \cdot \exp\left(-\frac{(t - t_n - 1.0)^2}{2 \cdot 0.5^2}\right). \quad (6)$$

PP2 is similar to **PP1**, except that E_1 events exert a delayed inhibitory effect on E_2 events:

$$\lambda_{E_1}(t|\mathcal{H}_t) = 0.5, \quad \lambda_{E_2}(t|\mathcal{H}_t) = \sigma\left[1.0 - \sum_{t_n < t, k_n = E_1} 1.5 \cdot \exp\left(-\frac{(t - t_n - 1.0)^2}{2 \cdot 0.5^2}\right)\right], \quad (7)$$

where $\sigma(x) = \frac{1}{\beta} \log(1 + \exp(\beta x))$ denotes the softplus transformation used to ensure non-negative intensity, with $\beta = 10$. We set the time horizon to $T = 50$ for **PP1** and $T = 40$ for **PP2**. For each process, we generated 6,000 independent sequences for training and 200 sequences for validation using Ogata’s thinning algorithm [Ogata, 1981].

We compared SNMPP with the following popular and state-of-the-art temporal point process models: (1) Multivariate Hawkes Process (MHP), which models excitation effects between event types using

an exponential triggering kernel; (2) Neural Hawkes Process (NHP) [Mei and Eisner, 2017], which encodes historical events via an LSTM and parameterizes the conditional intensity as a transformation of the hidden state; and (3) Transformer Hawkes Process (THP) [Zuo et al., 2020], which treats events as tokens, aggregates historical information through causal attention, and models the conditional intensity based on the resulting token representations. Our method is implemented in PyTorch and trained using the AdamW optimizer [Loshchilov and Hutter, 2019] with a learning rate of 10^{-3} . The mini-batch size is set to 128. Detailed hyperparameter settings are provided in Appendix D. We use the SoftPlus transformation with $\beta = 10$ in (1) to ensure non-negative conditional intensity. MHP is trained using Adam with the same learning rate. For the remaining baselines, we use the official open-source implementations with their default hyperparameter settings.

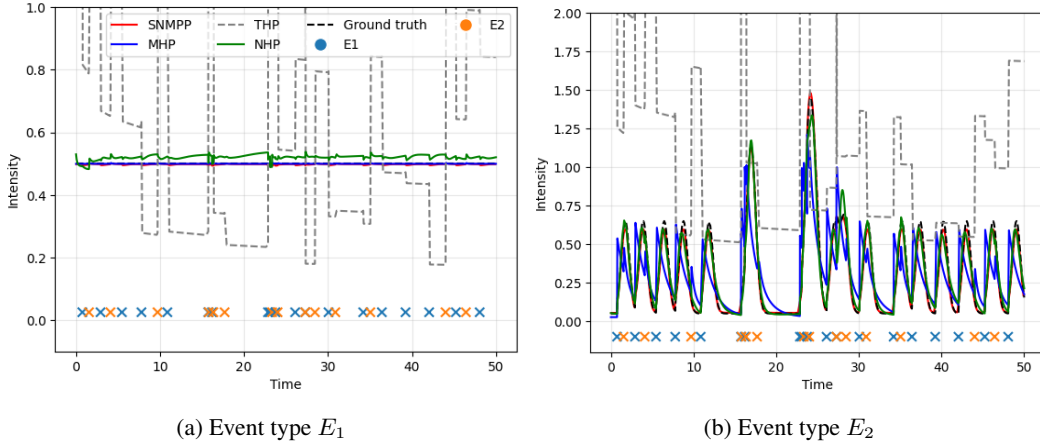


Figure 2: The conditional intensity function on a validation sequence from **PP1**.

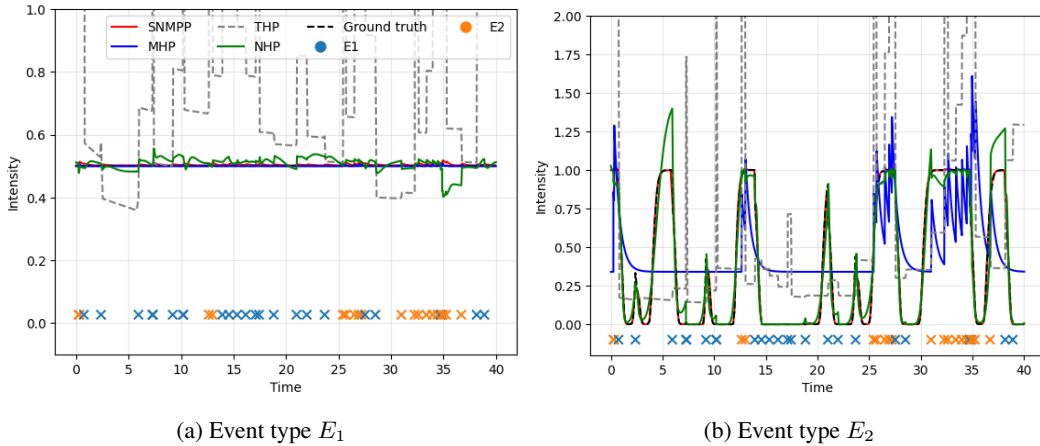


Figure 3: The conditional intensity function on a validation sequence from **PP2**.

Intensity Recovery. We first evaluated whether SNMPP can accurately recover the conditional intensity functions. For each of **PP1** and **PP2**, we randomly select one validation sequence and visualize the learned conditional intensity for each event type. As shown in Figures 2 and 3, SNMPP closely matches the ground-truth intensities, while THP exhibit substantial deviations. NHP approximates the intensity reasonably well, demonstrating its strong representational capacity. However, it is less accurate than SNMPP in capturing the complex temporal patterns of the E_2 intensity, particularly under delayed excitation and inhibition settings. MHP accurately recovers the E_1 intensity — which is constant and corresponds to a homogeneous Poisson process — in both **PP1** and **PP2**. This behavior is expected, as the Hawkes formulation reduces to a homogeneous Poisson process when excitation terms vanish. However, its estimation of the E_2 intensity deteriorates substantially — performing worse than NHP — especially for **PP2**, where inhibition dominates

the process. This highlights the limitations of standard Hawkes processes in modeling delayed or inhibitory dynamics. Importantly, although neural baselines such as NHP and THP can approximate the intensity function, they do *not* provide explicit or interpretable interaction structures, as event relationships remain embedded within latent representations.

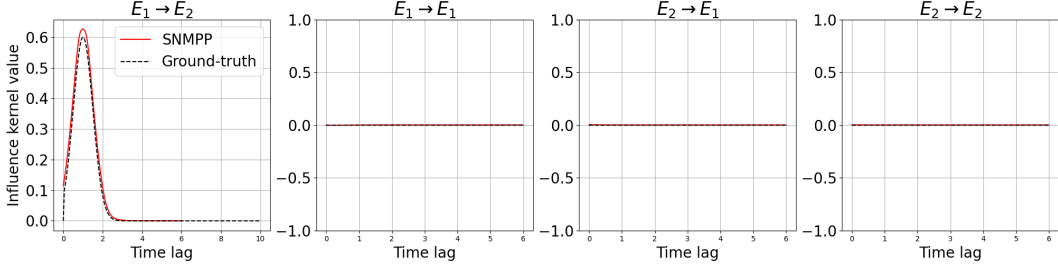


Figure 4: Learned influence kernel on **PP1**. Note that SNMPP learns a single unified influence kernel shared across all event types, as defined in (2).

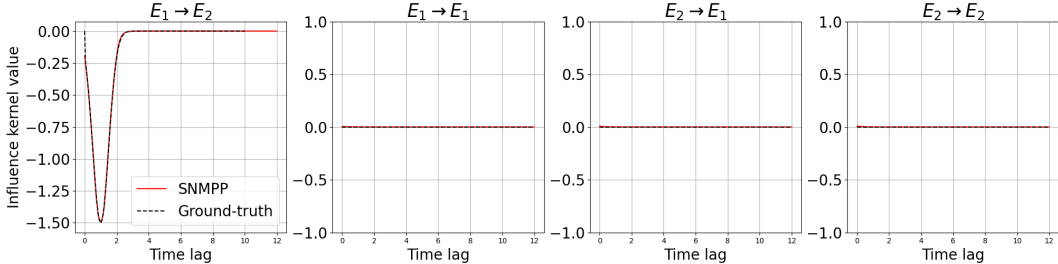


Figure 5: Learned influence kernel from **PP2**.

Structure Discovery. We then examined whether SNMPP can recover the interaction structure among event types and the temporal evolution of influence strengths. To this end, we visualize the learned influence functions for every ordered pair of event types. As shown in Figures 4 and 5, SNMPP not only correctly identifies the type of interaction — excitation, inhibition, or neutrality — but also accurately captures the temporal evolution of the influence strength.

In both **PP1** and **PP2**, the only true interaction is from E_1 to E_2 : a delayed excitation in **PP1** and a delayed inhibition in **PP2**. The learned influence function f closely matches the ground-truth kernel, including accurate estimation of the delay parameters. The estimated delays are 0.992 *versus* 1.0 for **PP1**, and 0.997 *versus* 1.0 for **PP2**.

For all other type pairs, including $E_1 \rightarrow E_1$, $E_2 \rightarrow E_2$, and $E_2 \rightarrow E_1$, there is no true interaction; the corresponding ground-truth kernels are identically zero. The learned kernels faithfully recover this null structure, with estimated delay parameters close to zero. In addition, SNMPP accurately estimates the baseline intensities for both processes. Detailed quantitative comparisons are provided in Appendix Table 2.

Overall, the results demonstrate that our *unified* neural influence kernel — despite being *shared* across all event-type pairs — can flexibly capture heterogeneous interaction patterns, distinguish delayed from non-delayed effects, and accurately recover delay parameters when present.

5.2 Predictive Performance

Next, we evaluated the predictive performance of SNMPP on five real-world benchmark datasets: **MIMIC** [Johnson et al., 2016], **Amazon** [McAuley and Ni, 2018], **Retweet** [Zhou et al., 2013], **Taxi** [Whong, 2014], and **StackOverflow** [Jure, 2014]. These datasets span diverse application domains, including medical visits, social network interactions, online shopping behavior, taxi pick-up and drop-off events, and online question–answering platforms. Detailed dataset descriptions and summary statistics are provided in Appendix C. For all datasets except MIMIC, we adopt the same training, validation, and test splits as provided in EasyTPP [Xue et al., 2024], an open-source benchmark suite offering standardized datasets and model implementations for temporal point

Table 1: Performance of next-event prediction on real-world datasets. Numbers in parenthesis indicates the standard deviation. *Results of SNMPP and the best result for each metric are shown in bold.*

MODEL	Metrics (Time RMSE/Type Error Rate)				
	Amazon	Retweet	Taxi	MIMIC	StackOverflow
MHP	0.635 / 75.9 % (0.005 / 0.005)	22.92 / 55.7 % (0.212 / 0.004)	0.382 / 9.53 % (0.002 / 0.0004)	0.839 / 31.7% (0.023 / 0.024)	1.388 / 65.0 % (0.011 / 0.005)
RMTTP	0.620 / 68.1% (0.005 / 0.006)	22.31 / 44.1% (0.209 / 0.003)	0.371 / 9.51% (0.003 / 0.0003)	0.950 / 50.3% (0.022 / 0.029)	1.376 / 57.3% (0.018 / 0.005)
NHP	0.621 / 67.1% (0.005 / 0.006)	21.90 / 40.0% (0.184 / 0.002)	0.369 / 8.50% (0.003 / 0.0005)	1.021 / 44.6% (0.028 / 0.031)	1.372 / 55.0% (0.011 / 0.006)
SAHP	0.619 / 67.7% (0.005 / 0.006)	22.40 / 41.6% (0.301 / 0.002)	0.372 / 9.75% (0.003 / 0.0008)	1.033 / 44.7% (0.023 / 0.026)	1.375 / 56.1% (0.013 / 0.005)
THP	0.621 / 66.1% (0.003 / 0.007)	22.01 / 41.5% (0.188 / 0.003)	0.370 / 8.68% (0.003 / 0.0006)	0.967 / 56.3% (0.020 / 0.028)	1.374 / 55.0% (0.021 / 0.006)
AttNHP	0.621 / 65.3% (0.005 / 0.006)	22.19 / 40.1% (0.180 / 0.003)	0.371 / 8.71% (0.003 / 0.0004)	0.975 / 33.0% (0.029 / 0.025)	1.372 / 55.2% (0.019 / 0.003)
ODETPP	0.620 / 65.8% (0.006 / 0.008)	22.48 / 43.2% (0.175 / 0.004)	0.371 / 10.54% (0.003 / 0.0008)	0.996 / 38.9% (0.063 / 0.064)	1.374 / 56.8% (0.022 / 0.004)
IFTTP	0.618 / 67.5% (0.005 / 0.007)	22.18 / 39.7% (0.204 / 0.003)	0.377 / 8.56% (0.003 / 0.006)	1.046 / 21.6% (0.078 / 0.029)	1.373 / 55.1% (0.010 / 0.005)
SNMPP	0.382 / 66.6% (0.001 / 0.002)	18.60 / 40.5% (0.122 / 0.001)	0.298 / 9.21% (0.010 / 0.006)	0.815 / 14.9 % (0.002 / 0.003)	1.05 / 56.2% (0.004 / 0.005)

processes. Since MIMIC is not included in EasyTPP, we use the data splits from widely adopted prior repositories [Mei and Eisner, 2017, Zuo et al., 2020]. Following [Xue et al., 2024], each experiment is repeated five times with different random initializations. We evaluated next-event time prediction using Root Mean Square Error (RMSE) and next-event type prediction using classification error rate, reporting the mean and standard deviation across runs.

In addition to the methods introduced in Section 5.1, we include: (4) Recurrent Marked Temporal Point Process (RMTTP) [Du et al., 2016], an RNN-based model that explicitly parameterizes the mark distribution; (5) Self-Attentive Hawkes Process (SAHP) [Zhang et al., 2020]; and (6) Attentive Neural Hawkes Process (AttNHP) [Yang et al., 2022], two additional attention-based models; (7) ODETPP [Chen et al., 2021], which combines neural ODE dynamics for continuous intensity evolution between events with GRU updates for event-triggered intensity jumps; and (8) IFTTP [Shchur et al., 2020], an intensity-free model that parameterizes inter-arrival time distributions instead of conditional intensities. EasyTPP provides state-of-the-art implementations of the competing models and performs systematic hyperparameter tuning based on validation performance. To ensure a fair comparison, we directly report their optimized results for these datasets. For MIMIC, we follow the same hyperparameter validation protocol described in [Xue et al., 2024]. For next-event time prediction, we use the posterior expectation under the learned conditional intensity. The expectation is evaluated via truncated numerical integration, with the truncation horizon set to five or ten times the empirical mean inter-event time of the training data. Detailed hyperparameter settings for SNMPP are provided in Appendix D.

As shown in Table 1, SNMPP consistently achieves the lowest time-prediction error across all datasets. While its event-type prediction accuracy is not always the highest, it remains consistently competitive and close to the best-performing methods. Notably, SNMPP consistently outperforms RMTTP in event-type prediction and achieves accuracy comparable to, or better than, NHP, SAHP, and THP.

Overall, these results show that our neural marked point process, despite explicitly modeling structured interaction topology and temporal influence dynamics, does not compromise predictive performance. On the contrary, SNMPP achieves state-of-the-art time-prediction accuracy among the compared methods. One possible explanation is that the proposed structured parameterization provides an effective inductive bias, regularizing the learning problem and improving temporal generalization. We provide a more detailed discussion of the expressivity–interpretability trade-off in Appendix G.

5.3 Supply-Chain System Simulation

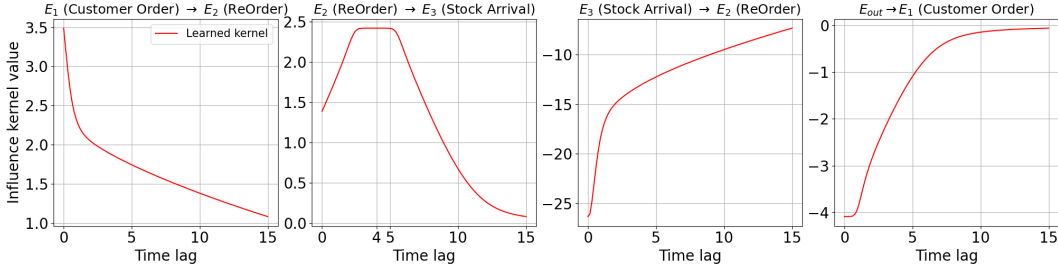


Figure 6: Influence kernels learned by SNMPP on event data generated by a simulated supply-chain system.

Third, we evaluated SNMPP on a simulated supply-chain system designed to reflect realistic operational logic. The event sequences are generated from stochastic dynamics governed by physical constraints and inventory decision rules, rather than being derived from any temporal point process model. This setting enables us to assess the robustness of our approach under misspecification — a common scenario in real-world applications — and to examine whether SNMPP can still recover critical interaction patterns, temporal dynamics, and underlying operational mechanisms.

Specifically, the simulator is implemented as a hidden-state inventory process that captures a closed-loop inventory workflow with four event types: customer orders (E_1), replenishment orders (E_2), stock arrivals (E_3), and a recorded stockout event (E_{out}). Customer orders E_1 are generated as candidate arrivals of a homogeneous Poisson process with a rate sampled uniformly from $[1.5, 3.5]$ over a time horizon $T_{max} = 30$. Each valid order decreases the (hidden) inventory by one unit. When the inventory first reaches zero, a stockout event E_{out} is recorded, and thereafter customer orders are physically suppressed (i.e., not recorded) until inventory is replenished. When the inventory falls below the reorder threshold $r = 5$ and no restock is pending, a replenishment order E_2 is triggered, which schedules a delayed stock arrival E_3 after a stochastic lead time sampled as $L = \max(0.5, \mathcal{N}(4.0, 1))$. Upon arrival, the inventory increases by a fixed quantity $q = 15$, and the stockout state is cleared. The initial inventory is set to 10. Full simulation details are provided in Appendix Section E. Our model is trained solely on the observed event timestamps and types, without access to the underlying hidden inventory state. We generate 1,500 sequences for training and 250 sequences for validation.

We first examined whether SNMPP can recover the interaction structure induced by the simulator (see Appendix E.4). We visualize the learned influence kernels for $E_1 \rightarrow E_2$, $E_2 \rightarrow E_3$, $E_3 \rightarrow E_2$, and $E_{out} \rightarrow E_1$. As shown in Figure 6, SNMPP correctly identifies the interaction types in all the cases. Customer orders (E_1) exhibit excitation on replenishment orders (E_2) due to inventory consumption. Replenishment orders (E_2) further excite stock arrival events (E_3). In contrast, stock arrival (E_3) inhibits replenishment orders (E_2) by restoring inventory. Finally, stock-out events (E_{out}) strongly inhibit customer orders (E_1), reflecting the physical constraint that no purchase can occur when inventory is depleted.

Notably, SNMPP accurately detects the *delayed* excitation from E_2 to E_3 . As shown in Figure 6 (second plot), the temporal influence for $E_2 \rightarrow E_3$ peaks near a time lag of 4.0 — with an estimated delay parameter of 3.92 — exhibiting a gradual increase followed by decay. This closely matches the simulation mechanism, where lead time is sampled from $L = \max(0.5, \mathcal{N}(4.0, 1))$. In practical supply chain systems, such delayed excitation is well understood: *manufacturing and transportation processes introduce inherent latency, so replenishment orders do not immediately translate into stock arrivals*. For the other interaction pairs, SNMPP captures immediate decaying patterns without delay, consistent with the simulation design. For example, the inhibitory effect of stock-out events (E_{out}) on customer orders (E_1) is instantaneous due to physical constraints.

We further visualize the intensity curve for E_1 (customer orders) on a validation sequence (Appendix Figure 7). The learned intensity reflects both the stochastic dynamics and underlying physical rules. Prior to any E_{out} event, the intensity fluctuates within $[1.5, 3.5]$, consistent with the simulation that generates E_1 events via a Poisson process with rate uniformly sampled from this range. Upon the occurrence of an E_{out} event, the intensity of E_1 drops sharply toward zero, reflecting the inability to place orders when inventory is exhausted. Conversely, once a stock arrival event (E_3) occurs, the

intensity immediately returns to the baseline range, indicating that customer demand resumes upon replenishment.

Overall, these results demonstrate that SNMPP successfully recovers the interaction topology, delay structure, inhibitory effects, and hard gating behavior embedded in the simulator, highlighting its potential for interpretable relationship discovery in real-world systems.

6 Conclusion

We presented SNMPP, a structured neural marked point process for multi-class event streams. Our model introduces a neural influence kernel that explicitly captures inter-type influence topology and event-wise temporal influence dynamics, while allowing flexible interaction signs, temporal decay patterns, and delayed effects. Across synthetic datasets, simulated dynamical systems, and real-world benchmarks, SNMPP demonstrates strong performance in both structured relationship discovery and prediction. Future work will extend the model to asymmetric temporal influence kernels and validate it on broader real-world applications; see Appendix G for further discussion.

References

- Charles Blundell, Jeff Beck, and Katherine A Heller. Modelling reciprocating relationships with Hawkes processes. In *Advances in Neural Information Processing Systems*, pages 2600–2608, 2012.
- Stephen Boyd and Lieven Vandenberghe. *Convex Optimization*. Cambridge University Press, 2004.
- Wei-Shiun Chang and Yu-Ting Lin. The effect of lead-time on supply chain resilience performance. *Asia Pacific Management Review*, 24(4):298–309, 2019.
- Laurent Charlin, Rajesh Ranganath, James McInerney, and David M Blei. Dynamic Poisson factorization. In *Proceedings of the 9th ACM Conference on Recommender Systems*, pages 155–162, 2015.
- Ricky T. Q. Chen, Brandon Amos, and Maximilian Nickel. Neural spatio-temporal point processes. In *International Conference on Learning Representations*, 2021.
- Nan Du, Mehrdad Farajtabar, Amr Ahmed, Alexander J Smola, and Le Song. Dirichlet-Hawkes processes with applications to clustering continuous-time document streams. In *Proceedings of the 21th ACM SIGKDD International Conference on Knowledge Discovery and Data Mining*, pages 219–228. ACM, 2015.
- Nan Du, Hanjun Dai, Rakshit Trivedi, Utkarsh Upadhyay, Manuel Gomez-Rodriguez, and Le Song. Recurrent marked temporal point processes: Embedding event history to vector. In *Proceedings of the 22nd ACM SIGKDD International Conference on Knowledge Discovery and Data Mining*, pages 1555–1564, 2016.
- Prem Gopalan, Laurent Charlin, and David M Blei. Content-based recommendations with Poisson factorization. *Advances in neural information processing systems*, 27, 2014.
- Prem Gopalan, Jake M Hofman, and David M Blei. Scalable recommendation with hierarchical Poisson factorization. In *UAI*, pages 326–335, 2015.
- Jan Grandell. *Doubly stochastic Poisson processes*. Springer, 2006.
- Alan G Hawkes. Spectra of some self-exciting and mutually exciting point processes. *Biometrika*, 58(1):83–90, 1971.
- Jafar Heydari, Reza Baradaran Kazemzadeh, and S Kamal Chaharsooghi. A study of lead time variation impact on supply chain performance. *The International Journal of Advanced Manufacturing Technology*, 40(11):1206–1215, 2009.
- Sepp Hochreiter and Jürgen Schmidhuber. Long short-term memory. *Neural computation*, 9(8):1735–1780, 1997.

- Nick Holford. Pharmacodynamic principles and the time course of delayed and cumulative drug effects. *Translational and Clinical Pharmacology*, 26(2):56–59, 2018.
- Alistair EW Johnson, Tom J Pollard, Lu Shen, Li-wei H Lehman, Mengling Feng, Mohammad Ghassemi, Benjamin Moody, Peter Szolovits, Leo Anthony Celi, and Roger G Mark. MIMIC-III, a freely accessible critical care database. *Scientific data*, 3(1):1–9, 2016.
- Leskovec Jure. Snap datasets: Stanford large network dataset collection. Retrieved December 2021 from <http://snap.stanford.edu/data>, 2014.
- Gavin Kerrigan, Kai Nelson, and Padhraic Smyth. EventFlow: Forecasting temporal point processes with flow matching. In *The 29th International Conference on Artificial Intelligence and Statistics*, 2026. URL <https://openreview.net/forum?id=QXqKGOE2JW>.
- Jerald Franklin Lawless. Regression methods for poisson process data. *Journal of the American Statistical Association*, 82(399):808–815, 1987.
- Haitao Lin, Lirong Wu, Guojiang Zhao, Liu Pai, and Stan Z. Li. Exploring generative neural temporal point process. *Transactions on Machine Learning Research*, 2022. ISSN 2835-8856. URL <https://openreview.net/forum?id=NPfS5N3jbL>.
- Ilya Loshchilov and Frank Hutter. Decoupled weight decay regularization. In *International Conference on Learning Representations*, 2019.
- David Lüdke, Marin Bilovs, Oleksandr Shchur, Marten Lienen, and Stephan Günnemann. Add and thin: Diffusion for temporal point processes. *Advances in Neural Information Processing Systems*, 36:56784–56801, 2023.
- David Lüdke, Marten Lienen, Marcel Kollovich, and Stephan Günnemann. Edit-based flow matching for temporal point processes. In *The Fourteenth International Conference on Learning Representations*, 2026. URL <https://openreview.net/forum?id=FNf9IV1P2L>.
- Julian McAuley and Jianmo Ni. Amazon review data (2018). Retrieved May, 11:2018, 2018.
- Hongyuan Mei and Jason M Eisner. The neural hawkes process: A neurally self-modulating multivariate point process. In *Advances in Neural Information Processing Systems*, pages 6754–6764, 2017.
- Lesley Meng, Krzysztof Laudanski, Mariana Restrepo, Ann Huffenberger, and Christian Terwiesch. The impact of delayed symptomatic treatment implementation in the intensive care unit. In *Healthcare*, volume 10, page 35. MDPI, 2021.
- Yurii Nesterov. Smooth minimization of non-smooth functions. *Mathematical Programming*, 103: 127–152, 2005.
- Yosihiko Ogata. On lewis’ simulation method for point processes. *IEEE transactions on information theory*, 27(1):23–31, 1981.
- Takahiro Omi, Kazuyuki Aihara, et al. Fully neural network based model for general temporal point processes. In *Advances in Neural Information Processing Systems*, pages 2122–2132, 2019.
- Oleksandr Shchur, Marin Bilovs, and Stephan Günnemann. Intensity-free learning of temporal point processes. In *International Conference on Learning Representations*, 2020. URL <https://openreview.net/forum?id=Hyg0jhEYDH>.
- Joseph Sill. Monotonic networks. *Advances in neural information processing systems*, 10, 1997.
- Yichen Wang, Xiaojing Ye, Hongyuan Zha, and Le Song. Predicting user activity level in point processes with mass transport equation. In *Advances in Neural Information Processing Systems*, pages 1644–1654, 2017.
- Chris Whong. Foiling nyc’s taxi trip data. *FOILing NYCs Taxi Trip Data*. Np, 18:14, 2014.
- Hongteng Xu, Dixin Luo, Xu Chen, and Lawrence Carin. Benefits from superposed hawkes processes. In *International Conference on Artificial Intelligence and Statistics*, pages 623–631. PMLR, 2018.

- Siqiao Xue, Xiaoming Shi, Zhixuan Chu, Yan Wang, Hongyan Hao, Fan Zhou, Caigao JIANG, Chen Pan, James Y Zhang, Qingsong Wen, et al. Easytpp: Towards open benchmarking temporal point processes. In *The Twelfth International Conference on Learning Representations*, 2024.
- Chenghao Yang, Hongyuan Mei, and Jason Eisner. Transformer embeddings of irregularly spaced events and their participants. In *Proceedings of the Tenth International Conference on Learning Representations (ICLR)*, 2022.
- Jiasen Yang, Vinayak A Rao, and Jennifer Neville. Decoupling homophily and reciprocity with latent space network models. In *UAI*, 2017.
- Ruoxin Yuan and Guanhua Fang. Residual TPP: A unified lightweight approach for event stream data analysis. In *Forty-second International Conference on Machine Learning*, 2025.
- Qiang Zhang, Aldo Lipani, Omer Kirnap, and Emine Yilmaz. Self-attentive hawkes process. In *International Conference on Machine Learning*, pages 11183–11193. PMLR, 2020.
- Ke Zhou, Hongyuan Zha, and Le Song. Learning triggering kernels for multi-dimensional hawkes processes. In *International conference on machine learning*, pages 1301–1309. PMLR, 2013.
- Simiao Zuo, Haoming Jiang, Zichong Li, Tuo Zhao, and Hongyuan Zha. Transformer hawkes process. In *International Conference on Machine Learning*, pages 11692–11702. PMLR, 2020.

Appendix

A Differentiable Soft Clipping

To constrain the temporal response within a bounded range while preserving differentiability, we replace the hard projection

$$\text{clip}(x; a, b) = \min(\max(x, a), b)$$

with a smooth approximation based on the log-sum-exp relaxation of the max and min operators [Boyd and Vandenberghe, 2004, Nesterov, 2005].

Smooth Maximum and Minimum. The smooth approximation of $\max(x, a)$ is given by

$$\max(x, a) \approx s \log(e^{x/s} + e^{a/s}),$$

where $s > 0$ controls smoothness. As $s \rightarrow 0$, this expression converges pointwise to $\max(x, a)$.

Similarly, a smooth approximation of $\min(y, b)$ can be written as

$$\min(y, b) \approx y - s \log(e^{(y-b)/s} + 1).$$

As $s \rightarrow 0$, this converges pointwise to $\min(y, b)$.

Soft Clipping Construction. A fully compositional smooth approximation to $\min(\max(x, a), b)$ would apply the smooth minimum to the smooth maximum:

$$\begin{aligned} \tilde{y} &= s \log(e^{x/s} + e^{a/s}), \\ \text{clip}_s(x; a, b) &= \tilde{y} - s \log(e^{(\tilde{y}-b)/s} + 1). \end{aligned}$$

For computational simplicity and improved numerical stability, we adopt the slightly simplified form:

$$\text{clip}_s(x; a, b) = s \log(e^{x/s} + e^{a/s}) - s \log(e^{(x-b)/s} + 1). \quad (8)$$

Note that the second term uses x instead of \tilde{y} . We now show that this modification does not affect pointwise convergence to the hard clipping operator.

Convergence Analysis. We analyze the limit $s \rightarrow 0$ under three cases.

- **Case 1:** $x < a$.

As $s \rightarrow 0$,

$$s \log(e^{x/s} + e^{a/s}) \rightarrow a,$$

since $e^{a/s}$ dominates. Moreover, since $x - b < 0$,

$$s \log(e^{(x-b)/s} + 1) \rightarrow 0.$$

Therefore,

$$\text{clip}_s(x; a, b) \rightarrow a.$$

- **Case 2:** $a \leq x \leq b$.

As $s \rightarrow 0$,

$$s \log(e^{x/s} + e^{a/s}) \rightarrow x,$$

since $e^{x/s}$ dominates. Additionally, since $x - b \leq 0$,

$$s \log(e^{(x-b)/s} + 1) \rightarrow 0.$$

Thus,

$$\text{clip}_s(x; a, b) \rightarrow x.$$

- **Case 3:** $x > b$.

As $s \rightarrow 0$,

$$s \log(e^{x/s} + e^{a/s}) \rightarrow x.$$

Since $x - b > 0$,

$$s \log(e^{(x-b)/s} + 1) \rightarrow x - b.$$

Therefore,

$$\text{clip}_s(x; a, b) \rightarrow x - (x - b) = b.$$

Conclusion. In all three cases,

$$\lim_{s \rightarrow 0} \text{clip}_s(x; a, b) = \min(\max(x, a), b).$$

Hence, although the second smooth term uses x instead of the smooth maximum \tilde{y} , the pointwise convergence to the hard projection remains unchanged. This simplification yields a computationally efficient and numerically stable implementation while preserving differentiability.

In our implementation, we set $a = 0$ and $b = 1$ to constrain the temporal decay component within $[0, 1]$, ensuring bounded influence magnitudes during training. We set the smooth hyperparameter $s = 0.1$.

B Variance Reduction of the Stratified Monte Carlo Estimator

We provide a variance-reduction justification for the stratified Monte Carlo estimator used in Section 3.2. Consider an inter-event interval $[t_n, t_{n+1}]$ and define its length as

$$L_n = t_{n+1} - t_n.$$

Since no event occurs inside this interval, the event history remains fixed within the interval. Therefore, for any fixed model parameters, the integrated intensity term can be written as an integral of a deterministic function over this interval. For example, for a single event type k , we may define

$$g(t) = \lambda_k(t \mid \mathcal{H}_{t_{n+1}}), \quad t \in [t_n, t_{n+1}],$$

or, for the full integrated intensity over all event types, we may define

$$g(t) = \sum_{k=1}^K \lambda_k(t \mid \mathcal{H}_{t_{n+1}}).$$

Thus, it suffices to analyze the estimation of

$$I = \int_{t_n}^{t_{n+1}} g(t) dt.$$

Partition $[t_n, t_{n+1}]$ into Q equal-length, non-overlapping subintervals S_1, \dots, S_Q , each of length L_n/Q . The stratified Monte Carlo estimator draws one sample $\hat{t}_q \sim \text{Unif}(S_q)$ from each subinterval and estimates

$$\hat{I}_{\text{strat}} = \frac{L_n}{Q} \sum_{q=1}^Q g(\hat{t}_q).$$

For comparison, the standard Monte Carlo estimator with the same number of samples draws $\tilde{t}_1, \dots, \tilde{t}_Q \stackrel{\text{i.i.d.}}{\sim} \text{Unif}([t_n, t_{n+1}])$ and estimates

$$\hat{I}_{\text{mc}} = \frac{L_n}{Q} \sum_{q=1}^Q g(\tilde{t}_q).$$

Lemma B.1 (Variance reduction of stratified Monte Carlo). *Assume $g(t)$ has finite second moment on $[t_n, t_{n+1}]$. Then both \hat{I}_{strat} and \hat{I}_{mc} are unbiased estimators of*

$$I = \int_{t_n}^{t_{n+1}} g(t) dt.$$

Moreover,

$$\text{Var}[\hat{I}_{\text{strat}}] \leq \text{Var}[\hat{I}_{\text{mc}}].$$

The inequality is strict whenever the stratum-wise means of g are not all identical.

Proof. We first show unbiasedness. For the stratified estimator,

$$\mathbb{E}[\widehat{I}_{\text{strat}}] = \frac{L_n}{Q} \sum_{q=1}^Q \mathbb{E}_{\hat{t}_q \sim \text{Unif}(S_q)}[g(\hat{t}_q)].$$

Since each S_q has length L_n/Q ,

$$\mathbb{E}_{\hat{t}_q \sim \text{Unif}(S_q)}[g(\hat{t}_q)] = \frac{Q}{L_n} \int_{S_q} g(t) dt.$$

Therefore,

$$\mathbb{E}[\widehat{I}_{\text{strat}}] = \frac{L_n}{Q} \sum_{q=1}^Q \frac{Q}{L_n} \int_{S_q} g(t) dt = \sum_{q=1}^Q \int_{S_q} g(t) dt = \int_{t_n}^{t_{n+1}} g(t) dt = I.$$

Similarly, for the standard Monte Carlo estimator,

$$\mathbb{E}[\widehat{I}_{\text{mc}}] = \frac{L_n}{Q} \sum_{q=1}^Q \mathbb{E}_{\hat{t}_q \sim \text{Unif}([t_n, t_{n+1}])}[g(\hat{t}_q)] = L_n \cdot \frac{1}{L_n} \int_{t_n}^{t_{n+1}} g(t) dt = I.$$

We now compare the variances. Define the stratum-wise mean and variance as

$$\mu_q = \mathbb{E}[g(\hat{t}_q) \mid \hat{t}_q \in S_q], \quad \sigma_q^2 = \text{Var}[g(\hat{t}_q) \mid \hat{t}_q \in S_q].$$

Since the samples $\hat{t}_1, \dots, \hat{t}_Q$ are independent across strata,

$$\text{Var}[\widehat{I}_{\text{strat}}] = \text{Var}\left[\frac{L_n}{Q} \sum_{q=1}^Q g(\hat{t}_q)\right] = \frac{L_n^2}{Q^2} \sum_{q=1}^Q \sigma_q^2.$$

For the standard Monte Carlo estimator, let $\tilde{t} \sim \text{Unif}([t_n, t_{n+1}])$. Drawing \tilde{t} uniformly from the whole interval is equivalent to first drawing a stratum index $J \sim \text{Unif}(\{1, \dots, Q\})$ and then drawing $\tilde{t} \sim \text{Unif}(S_J)$. By the law of total variance,

$$\text{Var}[g(\tilde{t})] = \mathbb{E}[\text{Var}(g(\tilde{t}) \mid J)] + \text{Var}(\mathbb{E}[g(\tilde{t}) \mid J]).$$

Using the definitions of μ_q and σ_q^2 , we obtain

$$\mathbb{E}[\text{Var}(g(\tilde{t}) \mid J)] = \frac{1}{Q} \sum_{q=1}^Q \sigma_q^2,$$

and

$$\text{Var}(\mathbb{E}[g(\tilde{t}) \mid J]) = \frac{1}{Q} \sum_{q=1}^Q (\mu_q - \bar{\mu})^2, \quad \bar{\mu} = \frac{1}{Q} \sum_{q=1}^Q \mu_q.$$

Therefore,

$$\text{Var}[g(\tilde{t})] = \frac{1}{Q} \sum_{q=1}^Q \sigma_q^2 + \frac{1}{Q} \sum_{q=1}^Q (\mu_q - \bar{\mu})^2.$$

Since \widehat{I}_{mc} averages Q i.i.d. samples from the full interval,

$$\text{Var}[\widehat{I}_{\text{mc}}] = \frac{L_n^2}{Q} \text{Var}[g(\tilde{t})].$$

Substituting the expression above gives

$$\text{Var}[\widehat{I}_{\text{mc}}] = \frac{L_n^2}{Q^2} \sum_{q=1}^Q \sigma_q^2 + \frac{L_n^2}{Q^2} \sum_{q=1}^Q (\mu_q - \bar{\mu})^2.$$

Comparing this with the variance of the stratified estimator yields

$$\text{Var}[\hat{I}_{\text{mc}}] = \text{Var}[\hat{I}_{\text{strat}}] + \frac{I_n^2}{Q^2} \sum_{q=1}^Q (\mu_q - \bar{\mu})^2.$$

The second term is nonnegative, and hence

$$\text{Var}[\hat{I}_{\text{strat}}] \leq \text{Var}[\hat{I}_{\text{mc}}].$$

The inequality is strict whenever the stratum-wise means μ_1, \dots, μ_Q are not all equal. \square

Lemma B.1 shows that standard Monte Carlo contains both within-stratum variability and between-stratum variability. In contrast, stratified Monte Carlo removes the between-stratum component by forcing one sample to be drawn from each subinterval. This is particularly useful when the conditional intensity varies systematically over an inter-event interval. In such cases, uniform sampling over the entire interval may concentrate samples in limited regions, whereas stratification enforces coverage across the interval and better captures local variation of the intensity function.

The same argument applies to the full likelihood integral by choosing $g(t) = \sum_{k=1}^K \lambda_k(t | \mathcal{H}_{t_{n+1}})$ on each interval. Moreover, under standard differentiability and finite-variance conditions, the same variance-reduction intuition also applies componentwise to stochastic gradient estimates, since gradients of the integral terms can be written as integrals of the corresponding derivative functions.

C Dataset Details

- **MIMIC** [Johnson et al., 2016]. This dataset contains de-identified ICU clinical visit records spanning seven years. Each visit is treated as an event, and the diagnosis category defines the event type, resulting in $K = 75$ types. The average sequence length is 3. We use 527 sequences for training, 58 for validation, and 65 for testing.
- **Amazon** [McAuley and Ni, 2018]. This dataset consists of time-stamped user product review events from January 2008 to October 2018. Each event corresponds to a reviewed product category, yielding $K = 16$ event types. We extract 5,200 active users, resulting in 6,454 training, 922 validation, and 1,851 test sequences. The average sequence length is 45 (minimum 14, maximum 94).
- **Retweet** [Zhou et al., 2013]. This dataset contains time-stamped retweet sequences categorized into $K = 3$ types: “small,” “medium,” and “large” users, defined by follower counts. We use 9,000 sequences for training, 1,535 for validation, and 1,520 for testing. The average sequence length is 41, with a maximum of 97.
- **Taxi** [Whong, 2014]. This dataset records time-stamped taxi pick-up and drop-off events across the five boroughs of New York City. Each (borough, pick-up/drop-off) pair defines an event type, yielding $K = 10$ types. We randomly sample 2,000 drivers and split them into 1,400 training, 200 validation, and 400 test sequences.
- **StackOverflow** [Jure, 2014]. This dataset contains two years of user badge-award events from a question-answering platform, with $K = 22$ badge types. The train/validation/test split is 4,066 / 451 / 1,126 sequences. The average sequence length is 59.

The MIMIC dataset was obtained from <https://drive.google.com/drive/folders/1DJZjYv1eWcmK55xmRk4jVRSB1A1x3vY4>, as provided in [Mei and Eisner, 2017, Zuo et al., 2020]. All other datasets were downloaded from the EasyTPP repository at <https://drive.google.com/drive/u/0/folders/1f8k82-NL6KFKuNMsUwozmbzDSFycYvz7>.

D Hyperparameter Settings

Throughout the experiments, we set the event-type embedding dimension to 4, the smooth parameter for the soft-clipping transformation $s = 0.1$, and the learning rate to 10^{-3} . For the interaction network ψ , we used the GELU activation function. For the monotonic temporal network ϕ , we adopted the SoftPlus activation (with $\beta = 1$) and enforced non-negativity of the linear weights by applying a

SoftPlus transformation to the unconstrained parameters. We set the number of segments to $Q = 4$ for the stratified Monte Carlo estimator. We evaluated $Q \in \{1, 2, 4\}$ and observed comparable final performance across all settings; however, $Q = 4$ exhibits slightly faster progress during the early training phase and lower variability. See Section F.1 for the corresponding ablation study.

For the synthetic datasets **PP1** and **PP2**, as well as the simulated supply-chain dataset, both ψ and ϕ were fixed to two hidden layers with 16 neurons per layer. For the real-world datasets, we varied the number of hidden layers in $\{1, 2, 3\}$ and the number of neurons per layer in $\{4, 8, 16, 32\}$. The mini-batch size is set to 16. Empirically, two hidden layers with 16 neurons each consistently provided robust performance across datasets. On the real-world and supply-chain datasets, we used ELU-plus-one as the positive link function in (1) to ensure non-negativity of the conditional intensity. Real-world experiments were run on a Linux workstation with an NVIDIA H200 GPU, while synthetic experiments were run on a workstation with an NVIDIA RTX 4090 GPU.

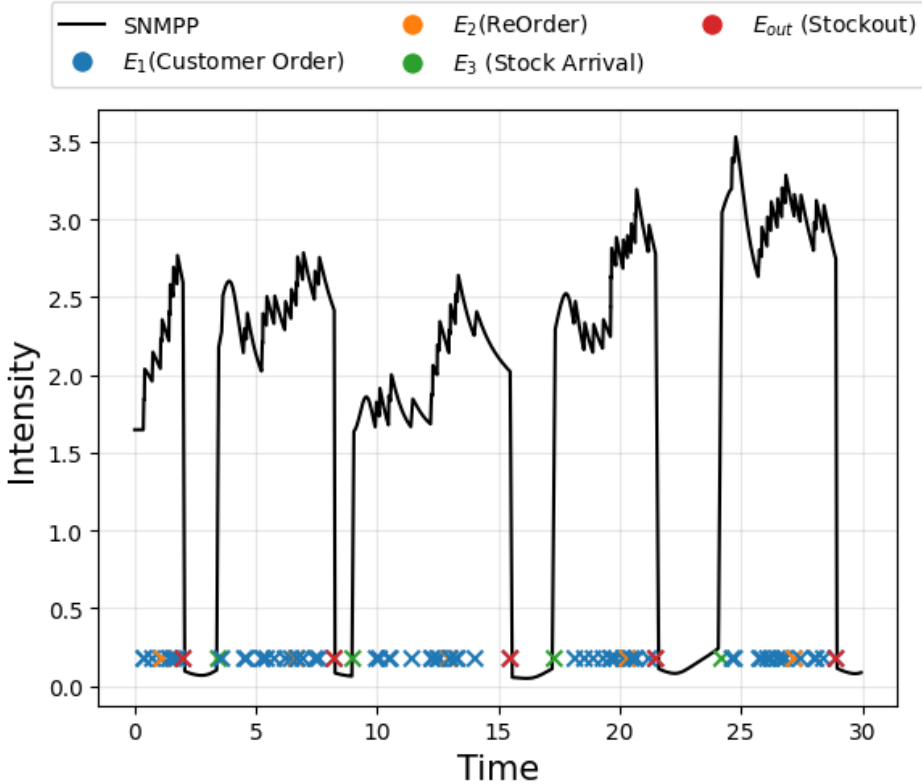


Figure 7: Conditional intensity function of E_1 (customer order) inferred by SNMPP on a sequence from the simulated supply-chain system.

E Supply-Chain System Simulation

We simulate event sequences using a hidden-state inventory generator that follows operational constraints and decision rules rather than a temporal point process. The model only observes the resulting event times and types.

E.1 Event types

The system produces four event types: (i) customer order E_1 , (ii) replenishment order E_2 , (iii) stock arrival E_3 , and (iv) recorded stockout E_{out} , which is emitted when inventory first reaches zero. Their physical meanings are summarized in Table 3.

Table 2: Base and delay parameter estimation on **PP1** and **PP2**.

(a) PP1						
	Base intensity (E_1)	Base intensity (E_2)	$d_{E_1 \rightarrow E_1}$	$d_{E_1 \rightarrow E_2}$	$d_{E_2 \rightarrow E_1}$	$d_{E_2 \rightarrow E_2}$
Ground-Truth	0.5	0.05	0	1.0	0	0
SNMPP	0.4982	0.0544	0.0011	0.9923	0.0045	0.0010

(b) PP2						
	Base intensity (E_1)	Base intensity (E_2)	$d_{E_1 \rightarrow E_1}$	$d_{E_1 \rightarrow E_2}$	$d_{E_2 \rightarrow E_1}$	$d_{E_2 \rightarrow E_2}$
Ground-Truth	0.5	1.0	0	1.0	0	0
SNMPP	0.5011	0.9999	0.0034	0.9970	0.0023	0.0002

Table 3: Event types in the supply-chain simulation.

Symbol	Event Type	Physical Meaning
E_1	Customer Order	Inventory consumption
E_2	Replenishment Order	Reaction to low inventory
E_3	Stock Arrival	Inventory restoration
E_{out}	Stockout Flag	Inventory reaches zero

E.2 Hidden state and parameters

The simulator maintains a hidden inventory level $I(t)$ and a pending restock arrival time t_{arr} (with at most one pending restock at any time). For each sequence, we initialize $I(0) = I_0$ and specify a reorder threshold r , reorder quantity q , mean lead time μ_L , and time horizon T_{max} .

The base demand rate is randomized independently for each sequence by sampling $\lambda \sim \text{Uniform}(1.5, 3.5)$. The remaining parameters are fixed as

$$T_{\text{max}} = 30, \quad I_0 = 10, \quad r = 5, \quad q = 15, \quad \mu_L = 4.0.$$

E.3 Dynamics and physical constraints

Candidate customer orders are generated by inter-arrival times $\Delta t \sim \text{Exp}(\lambda)$. A candidate order at time t becomes an observed E_1 only if $I(t^-) > 0$, in which case the inventory decreases by one. When the inventory first reaches zero, the simulator records a stockout event E_{out} and suppresses subsequent customer orders until the next stock arrival. When $I(t) \leq r$ and no restock is pending, a replenishment order E_2 is triggered and schedules a delayed arrival E_3 at time $t_{\text{arr}} = t + L$, where the lead time is sampled from a truncated normal distribution $L = \max(0.5, \mathcal{N}(\mu_L, 1))$. At E_3 , inventory increases by q , the pending flag is cleared, and the stockout state is reset.

E.4 Induced interaction structure

The generator yields:

- Excitation $E_1 \rightarrow E_2$ via inventory depletion.
- Delayed excitation $E_2 \rightarrow E_3$ via lead time.
- Inhibition $E_3 \rightarrow E_2$ through replenishment satisfaction (no new reorders while inventory is restored)
- Hard gating $E_{\text{out}} \rightarrow E_1$ by suppressing orders at zero inventory.

Algorithm 1 summarizes the simulation procedure.

Input: T_{\max} , I_0 , reorder point r , reorder quantity q , lead time mean μ_L
Sample demand rate $\lambda \sim \text{Uniform}(1.5, 3.5)$;
 $t \leftarrow 0, I \leftarrow I_0, t_{\text{arr}} \leftarrow \emptyset, \text{stockout} \leftarrow \text{false}$;
 $\Gamma \leftarrow []$;
while $t < T_{\max}$ **do**
 Sample $\Delta t \sim \text{Exp}(\lambda)$ and set $t_{E_1} \leftarrow t + \Delta t$;
 if $t_{\text{arr}} \neq \emptyset$ **and** $t_{\text{arr}} < t_{E_1}$ **then**
 $t \leftarrow t_{\text{arr}}$;
 Append (t, E_3) to Γ ;
 $I \leftarrow I + q, t_{\text{arr}} \leftarrow \emptyset, \text{stockout} \leftarrow \text{false}$;
 continue;
 end
 if $t_{E_1} > T_{\max}$ **then**
 | **break**
 end
 $t \leftarrow t_{E_1}$;
 if $I \leq 0$ **then**
 | // Hard gating: suppress customer orders during stockout
 | **continue**;
 end
 Append (t, E_1) to Γ ; $I \leftarrow I - 1$;
 if $I = 0$ **and** $\text{stockout} = \text{false}$ **then**
 | Append (t, E_{out}) to Γ ; $\text{stockout} \leftarrow \text{true}$;
 end
 if $I \leq r$ **and** $t_{\text{arr}} = \emptyset$ **then**
 | Append (t, E_2) to Γ ;
 | Sample $L \leftarrow \max(0.5, \mathcal{N}(\mu_L, 1))$;
 | $t_{\text{arr}} \leftarrow t + L$;
 end
end

Output: Chronologically ordered event sequence Γ

Algorithm 1: Supply-chain event simulation. In the experiments, we set $T_{\max} = 30$, $I_0 = 10$, $r = 5$, $q = 15$, and $\mu_L = 4.0$.

F Ablation Studies

F.1 Stratified Monte Carlo Estimator

Since the stratified Monte Carlo estimator is a central algorithmic component of our method, we conducted an ablation study on the number of stratification segments Q . Specifically, we used the StackOverflow (SO) dataset, varied $Q \in \{1, 2, 4\}$, and examined how the next-event time RMSE and event-type accuracy evolve during training.

In addition, we compared against a simple baseline that, for each sequence, randomly samples a single time point \hat{t} and approximates the likelihood integral over the entire sequence as

$$\int_0^T \lambda(t|\mathcal{H}_t) dt \approx T \cdot \lambda(\hat{t}|\mathcal{H}_{\hat{t}}). \quad (9)$$

We refer to this baseline as the *Global Monte Carlo Estimator* (GMCE). All methods use a learning rate of 10^{-3} and a mini-batch size of 16.

Comparison with GMCE. We first compared GMCE with our method using $Q = 1$. As shown in Figure 8, GMCE achieves a small time-prediction RMSE after the first epoch, but the error subsequently increases sharply before gradually decreasing and stabilizing. For event-type prediction, GMCE exhibits rapid initial improvement comparable to our method with $Q = 1$; however, after approximately 25 epochs, its performance begins to deteriorate. In contrast, our method demonstrates substantially more stable convergence behavior. This instability of GMCE is likely due to the significantly higher variance of the global estimator in (9), which approximates the entire integral

using a single sample, compared to our stratified estimator that approximates the integration over each inter-event interval (t_n, t_{n+1}) independently.

Effect of the Number of Segments Q . We next examined the learning curves of our method under different choices of Q . As shown in Figure 9, all choices of Q achieve comparable final predictive performance, with nearly identical validation-selected errors. However, larger Q values exhibit smoother learning curves and reduced variability during training. In particular, $Q = 4$ shows slightly faster improvement during the first 10 epochs. The learning curve with $Q = 1$ displays more frequent and larger fluctuations, while $Q = 2$ lies between the two ends. These results suggest that increasing the number of segments in the stratified Monte Carlo estimator reduces variance and improves training stability, while having limited impact on final predictive accuracy.

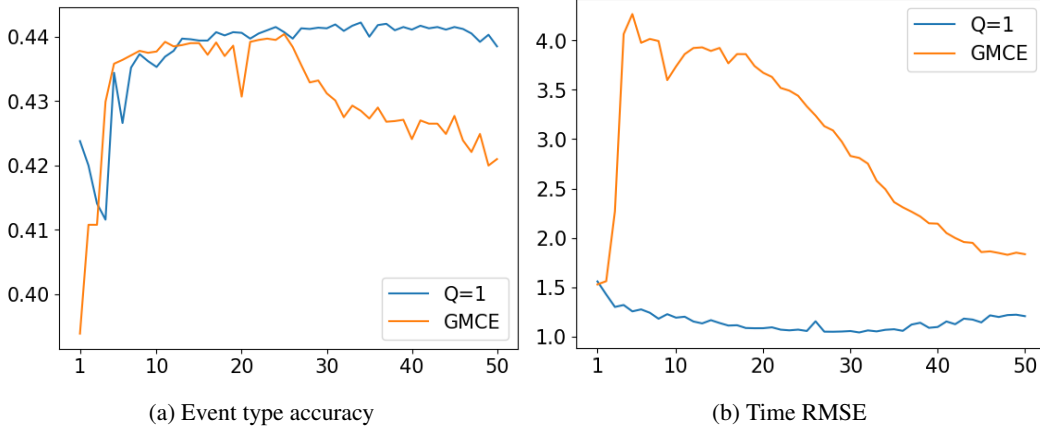


Figure 8: Next-event time RMSE and event-type prediction accuracy over training epochs for the global Monte Carlo estimator (GMCE) and our stratified Monte Carlo estimator ($Q = 1$).

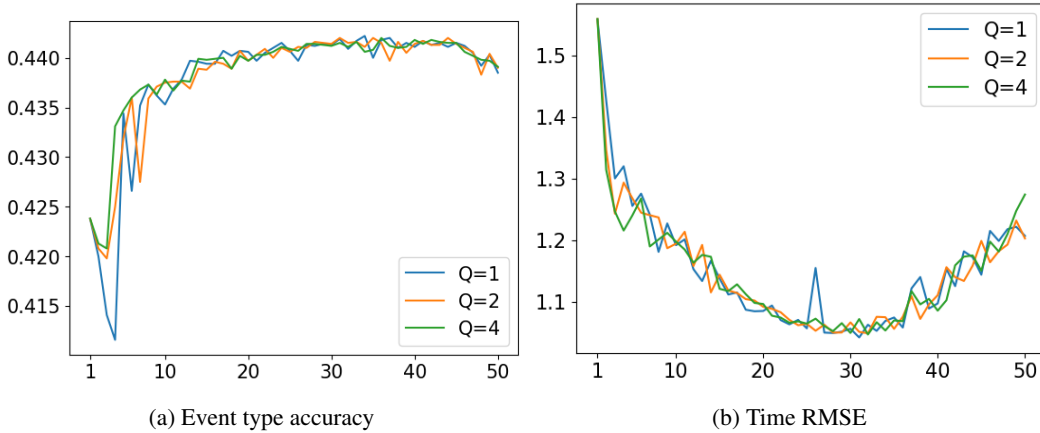


Figure 9: Next-event time RMSE and event-type prediction accuracy versus training epochs under different choices of Q .

F.2 Smoothness Parameter s

Throughout our experiments, we set the smoothness parameter to $s = 0.1$ in the soft-clipping transformation (3). In this section, we examine the sensitivity of SNMPP to this choice. We vary $s \in \{0.01, 0.05, 0.1, 0.5, 1.0, 10.0\}$ and evaluate SNMPP on the StackOverflow (SO) dataset. We track next-event type prediction accuracy and next-event time RMSE over training epochs.

As shown in Figure 10, all settings generally improve during training in both event-type and event-time prediction. However, the choice of s has a more pronounced effect on event-type prediction

accuracy than on event-time RMSE. In Figure 10a, larger values of s ($s \geq 0.5$) lead to substantial fluctuations in type accuracy after roughly 10 training epochs, with larger s values producing more unstable learning dynamics. In contrast, smaller values $s \in \{0.01, 0.05, 0.1\}$ yield more stable improvement throughout training. Among these settings, $s = 0.1$ is typically near the top of the accuracy curve, suggesting a slightly better stability–performance trade-off than smaller values.

For event-time prediction, the learning curves are less sensitive to s , as shown in Figure 10b. Nevertheless, very large values such as $s = 10.0$ still exhibit noticeable fluctuations after the early training phase. Overall, these results suggest that overly large smoothness values may make the soft-clipping transformation too diffuse, weakening the intended bounded-output behavior and leading to less stable optimization. The choice $s = 0.1$ provides a practical balance between smooth differentiability and effective clipping.

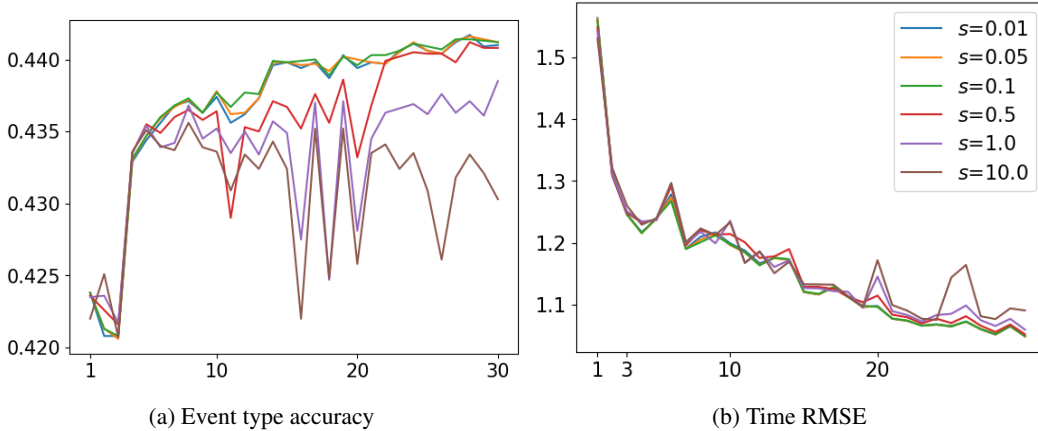


Figure 10: Next-event time RMSE and event-type prediction accuracy over training epochs with different choices of the smoothness parameter s in the soft-clipping transformation (3).

G Limitations, Discussion, and Future Work

SNMPP is designed to flexibly capture inter-type influence topology, diverse temporal decay patterns of event-level influence strength, and potential delayed peak effects. This structured design provides greater flexibility for interpretable relationship discovery than many classical temporal point process models, such as standard Hawkes processes. Nevertheless, the proposed structural inductive bias does not cover all possible temporal interaction patterns. For example, it may not fully capture multi-modal temporal influence profiles or interactions whose sign changes over time between the same pair of event types.

This limitation reflects a broader trade-off between expressivity and interpretability. Fully flexible black-box neural point process models can represent highly complex temporal dependencies, but their latent representations often obscure the underlying interaction structure. In contrast, overly restrictive structured models may fail to capture important dynamics. Our simulation studies in Section 5.1, together with empirical comparisons against black-box neural point process baselines, suggest that an appropriate inductive bias can improve interpretability while maintaining strong predictive performance. In particular, a model that is flexible enough to capture signed interactions with delayed and temporally decaying effects, while still being sufficiently structured to regularize the learning problem, can support more reliable relationship discovery from data.

An important direction for future work is to further expand the expressivity of our structured neural point processes while preserving interpretability. One natural extension is to allow asymmetric temporal influence profiles, where the influence trajectory before and after the estimated delay parameter is modeled by different neural components. Such a design could capture richer influence shapes around the delayed peak. However, it may also introduce additional training challenges, especially when many delay parameters are close to zero; in such cases, the network responsible for modeling the pre-delay influence region may receive limited training signal. A possible solution is

to first train a unimodal influence profile, as in the current model, and then fine-tune an additional asymmetric component. We leave this extension for future work.

NeurIPS Paper Checklist

The checklist is designed to encourage best practices for responsible machine learning research, addressing issues of reproducibility, transparency, research ethics, and societal impact. Do not remove the checklist: **The papers not including the checklist will be desk rejected.** The checklist should follow the references and follow the (optional) supplemental material. The checklist does NOT count towards the page limit.

Please read the checklist guidelines carefully for information on how to answer these questions. For each question in the checklist:

- You should answer [Yes], [No], or [N/A].
- [N/A] means either that the question is Not Applicable for that particular paper or the relevant information is Not Available.
- Please provide a short (1–2 sentence) justification right after your answer (even for [N/A]).

The checklist answers are an integral part of your paper submission. They are visible to the reviewers, area chairs, senior area chairs, and ethics reviewers. You will also be asked to include it (after eventual revisions) with the final version of your paper, and its final version will be published with the paper.

The reviewers of your paper will be asked to use the checklist as one of the factors in their evaluation. While [Yes] is generally preferable to [No], it is perfectly acceptable to answer [No] provided a proper justification is given (e.g., error bars are not reported because it would be too computationally expensive” or “we were unable to find the license for the dataset we used”). In general, answering [No] or [N/A] is not grounds for rejection. While the questions are phrased in a binary way, we acknowledge that the true answer is often more nuanced, so please just use your best judgment and write a justification to elaborate. All supporting evidence can appear either in the main paper or the supplemental material, provided in appendix. If you answer [Yes] to a question, in the justification please point to the section(s) where related material for the question can be found.

IMPORTANT, please:

- **Delete this instruction block, but keep the section heading “NeurIPS Paper Checklist”.**
- **Keep the checklist subsection headings, questions/answers and guidelines below.**
- **Do not modify the questions and only use the provided macros for your answers.**

1. Claims

Question: Do the main claims made in the abstract and introduction accurately reflect the paper’s contributions and scope?

Answer: [Yes]

Justification: Our abstract and introduction are align with our paper’s contributions and scope.

Guidelines:

- The answer [N/A] means that the abstract and introduction do not include the claims made in the paper.
- The abstract and/or introduction should clearly state the claims made, including the contributions made in the paper and important assumptions and limitations. A [No] or [N/A] answer to this question will not be perceived well by the reviewers.
- The claims made should match theoretical and experimental results, and reflect how much the results can be expected to generalize to other settings.
- It is fine to include aspirational goals as motivation as long as it is clear that these goals are not attained by the paper.

2. Limitations

Question: Does the paper discuss the limitations of the work performed by the authors?

Answer: [Yes]

Justification: We discussed the limitation in Section 6 and Appendix. G.

Guidelines:

- The answer [N/A] means that the paper has no limitation while the answer [No] means that the paper has limitations, but those are not discussed in the paper.
- The authors are encouraged to create a separate “Limitations” section in their paper.
- The paper should point out any strong assumptions and how robust the results are to violations of these assumptions (e.g., independence assumptions, noiseless settings, model well-specification, asymptotic approximations only holding locally). The authors should reflect on how these assumptions might be violated in practice and what the implications would be.
- The authors should reflect on the scope of the claims made, e.g., if the approach was only tested on a few datasets or with a few runs. In general, empirical results often depend on implicit assumptions, which should be articulated.
- The authors should reflect on the factors that influence the performance of the approach. For example, a facial recognition algorithm may perform poorly when image resolution is low or images are taken in low lighting. Or a speech-to-text system might not be used reliably to provide closed captions for online lectures because it fails to handle technical jargon.
- The authors should discuss the computational efficiency of the proposed algorithms and how they scale with dataset size.
- If applicable, the authors should discuss possible limitations of their approach to address problems of privacy and fairness.
- While the authors might fear that complete honesty about limitations might be used by reviewers as grounds for rejection, a worse outcome might be that reviewers discover limitations that aren’t acknowledged in the paper. The authors should use their best judgment and recognize that individual actions in favor of transparency play an important role in developing norms that preserve the integrity of the community. Reviewers will be specifically instructed to not penalize honesty concerning limitations.

3. Theory assumptions and proofs

Question: For each theoretical result, does the paper provide the full set of assumptions and a complete (and correct) proof?

Answer: [Yes]

Justification: Our theory and proof in Appendix. A and B provide the full set of assumptions and a complete and correct proof.

Guidelines:

- The answer [N/A] means that the paper does not include theoretical results.
- All the theorems, formulas, and proofs in the paper should be numbered and cross-referenced.
- All assumptions should be clearly stated or referenced in the statement of any theorems.
- The proofs can either appear in the main paper or the supplemental material, but if they appear in the supplemental material, the authors are encouraged to provide a short proof sketch to provide intuition.
- Inversely, any informal proof provided in the core of the paper should be complemented by formal proofs provided in appendix or supplemental material.
- Theorems and Lemmas that the proof relies upon should be properly referenced.

4. Experimental result reproducibility

Question: Does the paper fully disclose all the information needed to reproduce the main experimental results of the paper to the extent that it affects the main claims and/or conclusions of the paper (regardless of whether the code and data are provided or not)?

Answer: [Yes]

Justification: Our experiment results are reproducible with our code.

Guidelines:

- The answer [N/A] means that the paper does not include experiments.
- If the paper includes experiments, a [No] answer to this question will not be perceived well by the reviewers: Making the paper reproducible is important, regardless of whether the code and data are provided or not.
- If the contribution is a dataset and/or model, the authors should describe the steps taken to make their results reproducible or verifiable.
- Depending on the contribution, reproducibility can be accomplished in various ways. For example, if the contribution is a novel architecture, describing the architecture fully might suffice, or if the contribution is a specific model and empirical evaluation, it may be necessary to either make it possible for others to replicate the model with the same dataset, or provide access to the model. In general, releasing code and data is often one good way to accomplish this, but reproducibility can also be provided via detailed instructions for how to replicate the results, access to a hosted model (e.g., in the case of a large language model), releasing of a model checkpoint, or other means that are appropriate to the research performed.
- While NeurIPS does not require releasing code, the conference does require all submissions to provide some reasonable avenue for reproducibility, which may depend on the nature of the contribution. For example
 - (a) If the contribution is primarily a new algorithm, the paper should make it clear how to reproduce that algorithm.
 - (b) If the contribution is primarily a new model architecture, the paper should describe the architecture clearly and fully.
 - (c) If the contribution is a new model (e.g., a large language model), then there should either be a way to access this model for reproducing the results or a way to reproduce the model (e.g., with an open-source dataset or instructions for how to construct the dataset).
 - (d) We recognize that reproducibility may be tricky in some cases, in which case authors are welcome to describe the particular way they provide for reproducibility. In the case of closed-source models, it may be that access to the model is limited in some way (e.g., to registered users), but it should be possible for other researchers to have some path to reproducing or verifying the results.

5. Open access to data and code

Question: Does the paper provide open access to the data and code, with sufficient instructions to faithfully reproduce the main experimental results, as described in supplemental material?

Answer: [N/A]

Justification: We will release our code repository once our work is published.

Guidelines:

- The answer [N/A] means that paper does not include experiments requiring code.
- Please see the NeurIPS code and data submission guidelines (<https://neurips.cc/public/guides/CodeSubmissionPolicy>) for more details.
- While we encourage the release of code and data, we understand that this might not be possible, so [No] is an acceptable answer. Papers cannot be rejected simply for not including code, unless this is central to the contribution (e.g., for a new open-source benchmark).
- The instructions should contain the exact command and environment needed to run to reproduce the results. See the NeurIPS code and data submission guidelines (<https://neurips.cc/public/guides/CodeSubmissionPolicy>) for more details.
- The authors should provide instructions on data access and preparation, including how to access the raw data, preprocessed data, intermediate data, and generated data, etc.
- The authors should provide scripts to reproduce all experimental results for the new proposed method and baselines. If only a subset of experiments are reproducible, they should state which ones are omitted from the script and why.
- At submission time, to preserve anonymity, the authors should release anonymized versions (if applicable).

- Providing as much information as possible in supplemental material (appended to the paper) is recommended, but including URLs to data and code is permitted.

6. Experimental setting/details

Question: Does the paper specify all the training and test details (e.g., data splits, hyperparameters, how they were chosen, type of optimizer) necessary to understand the results?

Answer: [Yes]

Justification: The experiment settings and details are discussed in Appendix. D.

Guidelines:

- The answer [N/A] means that the paper does not include experiments.
- The experimental setting should be presented in the core of the paper to a level of detail that is necessary to appreciate the results and make sense of them.
- The full details can be provided either with the code, in appendix, or as supplemental material.

7. Experiment statistical significance

Question: Does the paper report error bars suitably and correctly defined or other appropriate information about the statistical significance of the experiments?

Answer: [Yes]

Justification: Our main results included standard deviation.

Guidelines:

- The answer [N/A] means that the paper does not include experiments.
- The authors should answer [Yes] if the results are accompanied by error bars, confidence intervals, or statistical significance tests, at least for the experiments that support the main claims of the paper.
- The factors of variability that the error bars are capturing should be clearly stated (for example, train/test split, initialization, random drawing of some parameter, or overall run with given experimental conditions).
- The method for calculating the error bars should be explained (closed form formula, call to a library function, bootstrap, etc.)
- The assumptions made should be given (e.g., Normally distributed errors).
- It should be clear whether the error bar is the standard deviation or the standard error of the mean.
- It is OK to report 1-sigma error bars, but one should state it. The authors should preferably report a 2-sigma error bar than state that they have a 96% CI, if the hypothesis of Normality of errors is not verified.
- For asymmetric distributions, the authors should be careful not to show in tables or figures symmetric error bars that would yield results that are out of range (e.g., negative error rates).
- If error bars are reported in tables or plots, the authors should explain in the text how they were calculated and reference the corresponding figures or tables in the text.

8. Experiments compute resources

Question: For each experiment, does the paper provide sufficient information on the computer resources (type of compute workers, memory, time of execution) needed to reproduce the experiments?

Answer: [Yes]

Justification: We discussed the hardware spec in Appendix. D.

Guidelines:

- The answer [N/A] means that the paper does not include experiments.
- The paper should indicate the type of compute workers CPU or GPU, internal cluster, or cloud provider, including relevant memory and storage.
- The paper should provide the amount of compute required for each of the individual experimental runs as well as estimate the total compute.

- The paper should disclose whether the full research project required more compute than the experiments reported in the paper (e.g., preliminary or failed experiments that didn't make it into the paper).

9. Code of ethics

Question: Does the research conducted in the paper conform, in every respect, with the NeurIPS Code of Ethics <https://neurips.cc/public/EthicsGuidelines?>

Answer: [Yes]

Justification: Our work follows NeurIPS Code of Ethics.

Guidelines:

- The answer [N/A] means that the authors have not reviewed the NeurIPS Code of Ethics.
- If the authors answer [No], they should explain the special circumstances that require a deviation from the Code of Ethics.
- The authors should make sure to preserve anonymity (e.g., if there is a special consideration due to laws or regulations in their jurisdiction).

10. Broader impacts

Question: Does the paper discuss both potential positive societal impacts and negative societal impacts of the work performed?

Answer: [N/A]

Justification: Our work does not have any societal impacts.

Guidelines:

- The answer [N/A] means that there is no societal impact of the work performed.
- If the authors answer [N/A] or [No], they should explain why their work has no societal impact or why the paper does not address societal impact.
- Examples of negative societal impacts include potential malicious or unintended uses (e.g., disinformation, generating fake profiles, surveillance), fairness considerations (e.g., deployment of technologies that could make decisions that unfairly impact specific groups), privacy considerations, and security considerations.
- The conference expects that many papers will be foundational research and not tied to particular applications, let alone deployments. However, if there is a direct path to any negative applications, the authors should point it out. For example, it is legitimate to point out that an improvement in the quality of generative models could be used to generate Deepfakes for disinformation. On the other hand, it is not needed to point out that a generic algorithm for optimizing neural networks could enable people to train models that generate Deepfakes faster.
- The authors should consider possible harms that could arise when the technology is being used as intended and functioning correctly, harms that could arise when the technology is being used as intended but gives incorrect results, and harms following from (intentional or unintentional) misuse of the technology.
- If there are negative societal impacts, the authors could also discuss possible mitigation strategies (e.g., gated release of models, providing defenses in addition to attacks, mechanisms for monitoring misuse, mechanisms to monitor how a system learns from feedback over time, improving the efficiency and accessibility of ML).

11. Safeguards

Question: Does the paper describe safeguards that have been put in place for responsible release of data or models that have a high risk for misuse (e.g., pre-trained language models, image generators, or scraped datasets)?

Answer: [N/A]

Justification: Our work poses no such risks.

Guidelines:

- The answer [N/A] means that the paper poses no such risks.

- Released models that have a high risk for misuse or dual-use should be released with necessary safeguards to allow for controlled use of the model, for example by requiring that users adhere to usage guidelines or restrictions to access the model or implementing safety filters.
- Datasets that have been scraped from the Internet could pose safety risks. The authors should describe how they avoided releasing unsafe images.
- We recognize that providing effective safeguards is challenging, and many papers do not require this, but we encourage authors to take this into account and make a best faith effort.

12. Licenses for existing assets

Question: Are the creators or original owners of assets (e.g., code, data, models), used in the paper, properly credited and are the license and terms of use explicitly mentioned and properly respected?

Answer: [N/A]

Justification: Our work does not use existing assets.

Guidelines:

- The answer [N/A] means that the paper does not use existing assets.
- The authors should cite the original paper that produced the code package or dataset.
- The authors should state which version of the asset is used and, if possible, include a URL.
- The name of the license (e.g., CC-BY 4.0) should be included for each asset.
- For scraped data from a particular source (e.g., website), the copyright and terms of service of that source should be provided.
- If assets are released, the license, copyright information, and terms of use in the package should be provided. For popular datasets, paperswithcode.com/datasets has curated licenses for some datasets. Their licensing guide can help determine the license of a dataset.
- For existing datasets that are re-packaged, both the original license and the license of the derived asset (if it has changed) should be provided.
- If this information is not available online, the authors are encouraged to reach out to the asset's creators.

13. New assets

Question: Are new assets introduced in the paper well documented and is the documentation provided alongside the assets?

Answer: [N/A]

Justification: Our work does not release new assets.

Guidelines:

- The answer [N/A] means that the paper does not release new assets.
- Researchers should communicate the details of the dataset/code/model as part of their submissions via structured templates. This includes details about training, license, limitations, etc.
- The paper should discuss whether and how consent was obtained from people whose asset is used.
- At submission time, remember to anonymize your assets (if applicable). You can either create an anonymized URL or include an anonymized zip file.

14. Crowdsourcing and research with human subjects

Question: For crowdsourcing experiments and research with human subjects, does the paper include the full text of instructions given to participants and screenshots, if applicable, as well as details about compensation (if any)?

Answer: [N/A]

Justification: Our work does not involve crowdsourcing nor research with human subjects.

Guidelines:

- The answer [N/A] means that the paper does not involve crowdsourcing nor research with human subjects.
- Including this information in the supplemental material is fine, but if the main contribution of the paper involves human subjects, then as much detail as possible should be included in the main paper.
- According to the NeurIPS Code of Ethics, workers involved in data collection, curation, or other labor should be paid at least the minimum wage in the country of the data collector.

15. Institutional review board (IRB) approvals or equivalent for research with human subjects

Question: Does the paper describe potential risks incurred by study participants, whether such risks were disclosed to the subjects, and whether Institutional Review Board (IRB) approvals (or an equivalent approval/review based on the requirements of your country or institution) were obtained?

Answer: [N/A]

Justification: Our work does not involve crowdsourcing nor research with human subjects.

Guidelines:

- The answer [N/A] means that the paper does not involve crowdsourcing nor research with human subjects.
- Depending on the country in which research is conducted, IRB approval (or equivalent) may be required for any human subjects research. If you obtained IRB approval, you should clearly state this in the paper.
- We recognize that the procedures for this may vary significantly between institutions and locations, and we expect authors to adhere to the NeurIPS Code of Ethics and the guidelines for their institution.
- For initial submissions, do not include any information that would break anonymity (if applicable), such as the institution conducting the review.

16. Declaration of LLM usage

Question: Does the paper describe the usage of LLMs if it is an important, original, or non-standard component of the core methods in this research? Note that if the LLM is used only for writing, editing, or formatting purposes and does *not* impact the core methodology, scientific rigor, or originality of the research, declaration is not required.

Answer: [N/A]

Justification: Our paper does not involve usage of LLM.

Guidelines:

- The answer [N/A] means that the core method development in this research does not involve LLMs as any important, original, or non-standard components.
- Please refer to our LLM policy in the NeurIPS handbook for what should or should not be described.